5
Solvent Detected NMR Approach for the Assessment of Solute-Solvent Interactions

5.1 INTRODUCTION

Analysis of solute-solvent interaction is not only important to predict the solubility of a certain chemical species but also attracts attention for deciphering various intermolecular forces responsible for the dynamic behaviour of the chemical substance in a solution. The interaction of the solute with the solvent molecules present in its immediate environment causes modification in physicochemical properties of the solute that further influences the interaction of solute molecules with other potential candidates in its vicinity. Therefore, selection of solvents plays an important role while deciphering molecular dynamics and interaction of a solute in the solution-state. The choice of solvent mixture rather than a pure solvent allows fine-tuning of the solvent properties for the system under investigation as discussed in section 1.5.3 (chapter 1). Fluoroalcohol : water mixtures are the most commonly used co-solvents to understand the solvation and conformational behavior of various proteins, peptides, and carbohydrates owing to fluoroalcohol's unique physicochemical properties as discussed in chapter 1 [Anderson and Webb, 2012; Chitra and Smith, 2001; Fioroni et al., 2002; Hong et al., 1999]. As an example 2, 2, 2-trifluoroethanol (TFE) : water co-solvent mixtures possessing unique ability to mimic the hydrophobic nature of biological systems can simulate cellular conditions. In this chapter we, therefore, aim to understand two such effects of TFE discussed in the literature: a) induction of structural transition in polypeptide chain; b) preferential solvation of a solute in aqueous media. In the following a brief review of literature is provided to present a cohesive idea of molecular interaction of TFE as a solvent in the two above mentioned cases.

5.1.1 Structural transition of Peptides in TFE cosolvent systems:

TFE-based co-solvents are well known for many decades to denature globular proteins and to stabilize secondary structures, in particular the open helices in peptides [Buck, 1998; Gast et al., 1999; Luo and Baldwin, 1997]. The effect of TFE on transition states and on the pathways of protein folding and unfolding has also been reviewed in the literature [Arthur et al., 2014; Carver and Collins, 1990; Díaz and Berger, 2001; Kentsis and Sosnick, 1998; Konno et al., 2000; Main and Jackson, 1999; Rajan and Balaram, 1996; Shao et al., 2012; Thomas and Dill, 1993]. Various hypotheses related to such observations are found in the literature which include the following: (i) TFE lowers the dielectric constant of aqueous solutions; (ii) it favors intermolecular hydrogen bonding; (iii) TFE promotes the preferential solvation of the peptide or protein; and (iv) it selectively interacts with the helical conformation of proteins [Jasanoff and Alan, 1994; Othon, et al., 2009]. Despite considerable discussions on the TFE induced structural transition of polypeptide chains, a cogent proposition related to a molecular mechanism accounting for all the effects of TFE and related co-solvents is still lacking. Hence, the interpretation of TFE titrations remains difficult till date [Cammers-goodwin et al., 1996]. Although the experimental evidence of polypeptide chain folding or structure induction is available, critical questions on the dynamical behaviour of TFE during such structure induction remain unanswered. Therefore, it is of interest to analyze the dynamics of TFE so that a generalised molecular mechanism for TFE and related co-solvent induced conformational changes in proteins and peptides can be proposed. The present chapter considers the solution behaviour of a model peptide melittin (MLT) in water-TFE co-solvent mixtures for deciphering the role of such chemical co-solvents during possible structural transitions of macromolecules.

MLT is known for unique structural transitions from random form to a fully folded tertiary structure [Kemple et al., 1997] making it a viable model for protein folding and aggregation studies [Liao et al., 2015]. It is an amphiphilic peptide containing 26 amino acid residues, with broad spectrum biological activities [Naumenkova et al., 2010]. It is also a major component of honey bee *Apis mellifera* venom [Roccatano et al., 2002] and is known to have potential antimicrobial property [Liao et al., 2015]. MLT exists as a random coil (unordered) monomer in water at low pH (acidic pH *i.e.* 2 to 5), or in solutions of low ionic strength at low peptide concentration [Othon et al., 2009; Yuan et al., 1996]. It can associate into α-helical tetramer that mimics small globular proteins under any one of the following conditions: (i) the pH is raised from 4.0 to 9.5; (ii) the ionic strength of the solution is increased; (iii) the temperature is raised or lowered from about 25°C–37°C; (iv) salt, ions and peptide concentration is raised [Wilcox and Eisenberg, 1992]. Also, in presence of alcohol it can take up α-helical conformation. Unlike most of the other proteins, the secondary structural units are not linked in the tetramer of MLT allowing observation of structural transition of MLT under various aforementioned physical conditions with ease [Wilcox and Eisenberg, 1992]. Research articles have discussed the effect of temperature, pH, concentration of peptide and concentration of salt on the reversible structural transition of MLT from a monomer to a self-aggregated/tetramer form by observing the changes in the proton NMR chemical shift and resonance line shapes [Miura, 2012, 2016]. Further, circular dichroism (CD) and fluorescence spectroscopy have been used to understand solvation (such as TFE) dynamics of MLT [Goto and Hagihara, 1992; Othon et al., 2009], besides experiments exploiting $^{19}F–^{1}H$ and $^{1}H–^{1}H$ NOE to comment on preferential solvation of MLT by TFE [Gerig, 2004; Neuman Jr and Gerig, 2009]. Molecular Dynamics (MD) simulation studies have revealed that helical conformation of MLT in alcohol are more stable than in aqueous solution [H. Liu and Hsu, 2003; Naumenkova et al., 2010]. The present chapter addresses aqueous MLT structural transition in the presence of TFE as a co-solvent.

5.1.2 Preferential solvation by TFE

In solvent mixtures, the specific interaction of solute molecules with one of the component of the solvent mixture over the other components results in differential composition of the solvent molecules in the immediate vicinity of solute (solvation sphere) than in the bulk (solvation bulk). This phenomenon is commonly addressed as preferential solvation in literature [Zhao et al., 2020] and is studied to infer valuable information regarding the kinetics and thermodynamics of essential processes [Rabinovitz, 1976]. The present chapter further, focusses to understand the solvation effect of TFE in a binary solvent mixture containing carbohydrates as the solute in specific. Due to the widespread involvement of carbohydrates and their derivatives in several biochemical and biophysical processes which take place in complex solvent media, they are recognized as an exciting systems to be investigated [Banipal et al., 2017]. The strong interactions of carbohydrates with solvents depict the ability of these molecules to undergo marked preferential solvation when dissolved into solvent mixture systems [Bagno et al., 2004; Vishnyakov and Laaksonen, 2000]. These interactions are generally non-covalent in nature [Herrera-castro and Torres, 2019]. Various methods such as calorimetry, infrared spectroscopy, molecular dynamics, adiabatic compressibility determined by ultrasonic velocity measurements and NMR are often exploited to analyze the solvation of different carbohydrates in the presence of water or various co-solvent mixtures [Boonyarattanakalin et al., 2015; Herrera-castro and Torres, 2019; Nomura et al., 1982; Saielli and Bagno, 2010; Shiio and Yoshihashi, 1956].

5.1.3 Methods in focus

Nuclear Overhauser enhancement (NOE) NMR experiments have emerged as one of the widely employed methods to investigate selective solvent-solute interactions for supramolecular (carbohydrates) as well as macromolecular systems (proteins and peptides) [Angulo and Berger, 2004; Gerig, 2004; Guerrero-Martínez et al., 2006; Halle, 2003; Mayer, 2002;

Sabadini et al., 2008]. However, two-dimensional (2D) NOESY (NOE SpectroscopY) experiments are often limited by the low sensitivity (signals of poor intensity and phase) owing to the intrinsic weakness of the observed intermolecular dipolar interactions between solute and solvent. The strong solvent signal further dampens the observation of intermolecular dipolar interactions between solute and solvent. Double pulsed field gradient spin-echo (DPFGSE) based 1D NOESY experiments have been proposed in the literature to partially overcome the aforementioned limitations by delivering high sensitivity [Bagno et al., 2004]. However, such an approach is far from the general application as it depends on the filtering efficiency of solute. The other viable methods to analyse solute-solvent interaction could be employment of relaxation analysis of either the solute or the solvent as highlighted in chapter 3 and 4. Nevertheless, the present chapter brings forth a refreshing change by highlighting the use of ^{19}F spin-lattice relaxation measurements both at high and low magnetic fields in conjunction with low field Overhauser dynamic nuclear polarization (ODNP) in case of MLT and heteronuclear ^{2}H relaxation analysis at high field in case of carbohydrates for analysing molecular interaction and dynamics of TFE in TFE: water co-solvent mixture. In both the cases, the ^{19}F NMR signal of the solvent (TFE) is directly monitored instead of the solute (MLT or β-CD or Glucose). The single ^{19}F chemical shift of TFE allowed us to avoid the spectral complexities observed in the ^{1}H NMR spectrum of the peptide or carbohydrates. Such an overcrowded complex nature of NMR spectra is a hindrance to obtain a clear insight into the dynamical characteristics of the MLT-TFE/H_2O or carbohydrates-TFE/H_2O system. It may be noted that low field ^{19}F relaxation measurements at *ca*. 0.34 T allow the system to satisfy the extreme narrowing condition even up to motional correlation times (τ_c) of *ca*. 552 ps, enabling direct extraction of correlation time (τ_c) from the measured relaxation rates of TFE considering dipole-dipole interaction as the only active relaxation mechanism.

In part I, we, for the first time, benchmark the low field ^{19}F relaxation and ^{19}F ODNP as viable ^{19}F MR approaches to analyse the solvent dynamics of TFE in the presence of the structural transitions of a model aqueous MLT solution at pH 7.4 with TFE as a co-solvent. Further, these two experimental approaches have been employed to elucidate TFE dynamics in a non-buffered solution of MLT at pH 2.8 for the first time. Our main focus is to shed light on the dynamical behavior of TFE during different conformational transitions of MLT in presence of TFE: D_2O co-solvent at different pH conditions. The specific emphasis is to understand the TFE dynamical behaviour in the solvation sphere of MLT in presence of such molecular transitions. Two different solvent conditions are chosen as mentioned in the Experimental Section, to explore the tetramer to monomer, and random coil to dense α-helical conformational transition of MLT under the influence of TFE. Till now, no reports are available where TFE dynamics have been analyzed during MLT structural transitions. Moreover, our literature survey indicates that NMR methods used to decipher the effect of variation of solvent composition (TFE and D_2O) at pH 2.8 on MLT's structural transitions (random coil to aggregate) have not been explored adequately. Therefore, the lack of NMR studies on TFE dynamics for the MLT-TFE system motivated us to attempt to establish a combination of low field relaxation and ODNP measurements to probe TFE dynamics during MLT–TFE interaction, especially to understand how the random coiled structure of peptide at low pH values is stabilized to secondary helical structure in presence of TFE. We believe that low field NMR relaxation and DNP measurements can provide the most direct and accurate quantitative data. The analysis of the DNP coupling parameter (ξ) from ODNP experiments provides complementary knowledge of solvent dynamics [Armstrong and Han, 2009], reflecting peptide aggregation by such a solvent. This proof of the concept study would add substantially to the understanding of the role of bulk and local solvent properties in the integrity of protein structure [Othon et al., 2009]. Figure 5.1 presents a graphical illustration of the same [Chaubey et. al., 2020a].

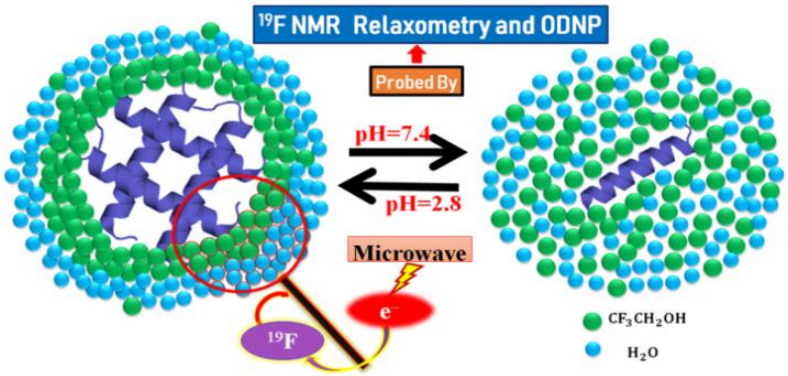

Figure 5.1: Graphical representation of the current investigation (part-I) showing structural transition of MLT in TFE: D_2O co-solvent system.

In the part II of the current chapter, the tendency of two carbohydrates *viz.*, β-cyclodextrin (β-CD) and D-glucose to undergo selective solvation by TFE in TFE: D_2O co-solvent mixture has been investigated. We have proposed a simpler solution focusing on NMR hetero nuclear relaxation (^{19}F and ^{2}H NMR R_1) analysis of solvent nuclei. This approach allows us to comment on the preferential solvation behavior of carbohydrates by analyzing solvent dynamics with higher sensitivity and significantly reduced machine time. β-CD is well known cyclic oligosaccharide made up of seven D-glucose units joined together through 1,4 glycosidic linkage [Sabadini et al., 2008]. Glucose molecules serve as monomer units for β-CD, (molecular structures are given in figure 5.2). β-CD and glucose are identified as model solutes to establish our approach as solvation of these systems have previously been taken into account in the presence of various co-solvent systems. The behavior of D_2O and trifluoroethanol (TFE) is monitored around β-CD (β-cyclodextrin) and glucose through spin-lattice relaxation rates, R_{1D} (^{2}H) and R_{1F} (^{19}F), respectively. Correlation times (τ_c) are determined for D_2O and TFE for various compositions of % (v/v) TFE: D_2O mixture. The differential trends of R_1 or τ_c ratio for D_2O and TFE (in presence & absence of carbohydrates) revealed that both β-CD and glucose undergo selective solvation by TFE over D_2O. Owing to its encapsulation property, β-CD exhibited a comparatively higher tendency for preferential solvation by TFE than glucose. It is also inferred that the maximum transfer of solute bound water to bulk solvent appears in 20–30% (v/v) TFE range. The current approach emerges straightforward in contrast to traditional methods that primarily focus on solute behavior to unravel the preferential solvation dynamics. Figure 5.3 presents a graphical illustration of the same.

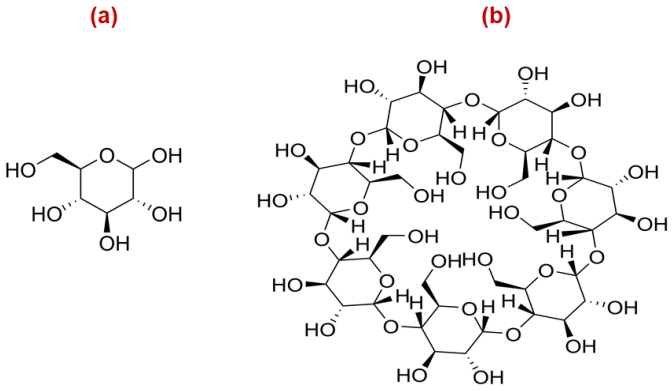

Figure 5.2: Molecular structure of (a) glucose (pyranose form) (b) β–Cyclodextrin (β–CD).

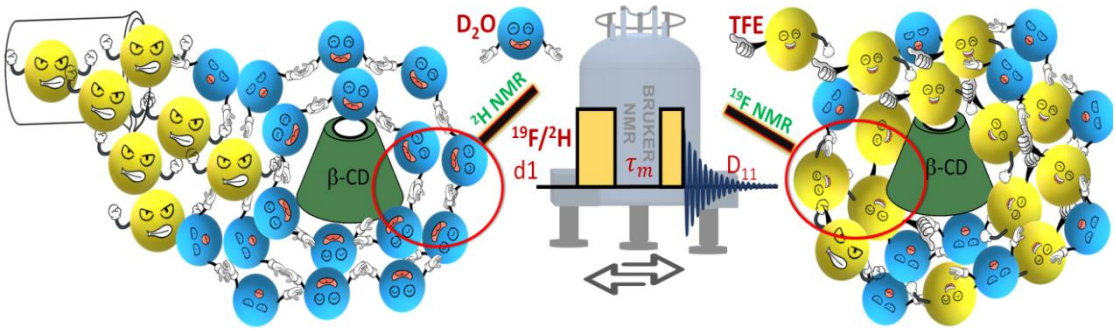

Figure 5.3: Graphical representation of the current investigation (Part-II) showing addition of TFE to aqueous β-CD solution causes replacement of D_2O from the solvation sphere of β-CD by TFE.

5.2 EXPERIMENTAL DETAILS

5.2.1 Solution Preparations:

Part I: For NMR experiments, two sets each of ten samples (set-I and set-II) are prepared. For set-I, stock solution of MLT (5 mM) is prepared by dissolving in a D_2O solution of 10 mM HEPES buffer and 0.5 M NaCl maintaining pD= 7.40. While for set-II, stock solution of MLT (5 mM) is prepared in D_2O only having a pD= 2.75. Ten samples are prepared for each set with varying TFE composition ranging from 2% (v/v) to 65% (v/v) with respect to D_2O. The relevant descriptions of the sample concentrations, components and pH for each set are presented in table 5.1.

Table 5.1: Description of samples of set-I and set-II. √: represents a sample prepared and used for recording NMR data.

	Set-I (D_2O solvent, 10 mM Hepes buffer, 0.5 M NaCl, pH=7.4)					Set-II (D_2O solvent, pH=2.75)					
Mellitin (mM)	TFE composition (%, v/v with respect to D_2O)					Mellitin (mM)	TFE composition (%, v/v with respect to D_2O)				
	2	10	20	42	65		2	10	20	42	65
0	√	√	√	√	√	0	√	√	√	√	√
1	√	√	√	√	√	1	√	√	√	√	√

Similar set of MLT samples (in absence and presence of buffer) are prepared for circular dichorism (CD) measurements. The pH of all the samples is determined using A255 Orion pH meter equipped with 5 mm o.d. micro-glass ROSS electrode.

Part II: Samples containing various compositions of TFE *i.e.* 2%, 5%, 10%, 20%, 30%, 42%, 65%, and 80% (v/v) TFE with respect to D_2O are prepared in absence and presence of 5 mM β-CD and 5 mM glucose.

Viscosity of the TFE-D_2O compositions in absence and presence of MLT or carbohydrates are determined with an Anton Paar MicroViscometer. The temperature is controlled at 25°C. For calibration the viscosity of distilled water at 25°C has been taken from the literature (η = 0.894 cP) as a reference [Adamson, 1979]. All the samples are equilibrated at room temperature and are degassed with nitrogen before measurements.

5.2.2 Technical Details

(i) Circular Dichroism Measurements: The CD spectra are recorded using JASCO J-815 CD-spectrometer in nitrogen (N_2) atmosphere in the wavelength range of 200–300 nm. An N_2 purging rate of 5 LPM (5 L/min) is maintained throughout the experiments. A scan rate of 20 nm / min is used.

(ii) NMR Measurements: ^{1}H and ^{19}F NMR measurements are carried out: (a) at 11.7 T (details mentioned in chapter 2, section 2.1); and (b) at 0.34 T (corresponding to *ca*. 13.7 MHz for ^{19}F and 14.6 MHz for ^{1}H). ^{19}F & ^{1}H R_1 are measured employing standard inversion recovery with a set of 20 recovery periods ranging from 50 µs to 45 s while for ^{2}H R_1 measurements, 20 recovery periods ranging from 50 µs to 10 s are used. The ^{19}F & ^{1}H R_2 is measured at 11.7 T (500 MHz) using CPMG pulse sequences employing a range of spin echo repetition loops $(\tau-\pi-\tau)_n$ from 2 to 5000 with single spin-echo delay (τ) of 2 ms.

(iii) **DNP measurements:** Overhauser DNP measurements are performed on a Bruker pulsed ELEXSYS system in conjunction with AVANCE III electronics respectively for MW and RF excitation and detection. Experiments are carried out with a coil-in-the-cavity configuration (Bruker MD4 resonator) employing tuning and matching boxes (tunable to either ^{19}F or ^{1}H) for NMR sensitivity and nuclear isotope selectivity in a Bruker wide air gap 10″ electromagnet with 2.7 kW power supply. The hardware has the capability to trigger microwave pulsing (ELEXSYS) from the NMR pulse program (AV III), and *vice versa*. MW irradiation, used to saturate the electron spin transitions prior to the RF pulses, is triggered from the NMR pulse sequence. The maximum microwave power output available is *ca*. 5 W with 100 % duty cycle at X-band (^{19}F and ^{1}H NMR frequency *ca*. 13.7 MHz and *ca*. 14.6 MHz respectively; EPR frequency *ca*. 9.6 GHz). All experiments have been performed at room temperature (*ca*. 298 K) in 1.6 mm o.d. sample tubes at X-band after degassing the samples with dry nitrogen gas. Pure dry nitrogen gas is also passed through the cavity, besides additional external cooling during the experiments.

5.3 RESULTS AND DISCUSSIONS:

5.3.1 Part I: Role of TFE solvent dynamics in inducing conformational transitions in MLT

(i) CD results: A series of CD measurements are performed initially to understand the native structure of MLT and structure induced in MLT by TFE in two solvents with different pH conditions. From the CD analysis it has been found that MLT exists as random coil in pure D_2O (0% v/v TFE). In set-I samples, MLT exists in the α-helical tetrameric form [Othon et al., 2009] that undergoes transition to open helical monomeric form with addition of TFE. It is well known in the literature that addition of TFE to the solution induces α-helicity in the polypeptide chain. For set-II samples, a similar effect is observed where random coiled MLT changes to highly dense α-helical state with increase in TFE concentration. These findings are further elaborated in the following.

(a) Set I: MLT in HEPES Buffer (10 mM) with 0.5 M NaCl, at pH 7.4: Effect of TFE composition

The pH of the solution governs the conformational state of MLT. It is well known that degree of aggregation of MLT increases with increasing pH as well as salt concentration of the solution. According to literature reports, in HEPES buffer solution with 0.5 M NaCl, MLT would be in tetramer conformation [Othon et al., 2009] that can be probed by CD. The set-I samples are analysed in terms of the molecular transition in order to validate our approach with respect to the existing studies in the literature. In general, a peptide in its fully helical form exhibits negative CD angles at 207 nm and 221 nm. This observation is characteristic of α-helical structure. Hence, it is expected that MLT in tetramer conformation (maximum helicity) will exhibit the highest negative CD angles at these two wavelengths. As can be seen from figure 5.4, the negative CD angles recorded at both the wavelengths are highest for 2% (v/v) TFE for set-I

samples, and decrease with increasing % (v/v) of TFE. This observation of decrement of CD angles suggests that the addition of TFE results in breaking of tetrameric/ self-aggregated form of MLT with a consequent decrease in α-helicity of the structure. The highest decrease is recorded in case of 65% (v/v) TFE concentration. Above this concentration (65% TFE) the CD angle recorded at 207 nm continues to decrease: however, the extent of change in CD angle is minimal. In case of set-I samples MLT remains folded with a tetrameric/self-aggregated form that resembles a globular protein [Kemple et al., 1997] not only in terms of structure but also in terms of its behaviour. Similar to the globular protein that denatures in a binary mixture of alcohol and water, MLT exhibits denaturation of the tetrameric/self-aggregated form with increasing TFE concentration. Hence, one may infer that in set-I samples, TFE denatures the tetrameric globular protein-like tertiary structure of MLT.

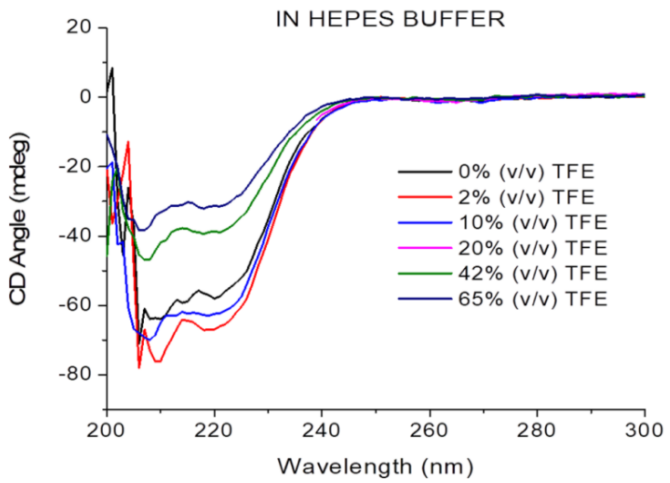

Figure 5.4: CD spectra of MLT in set-I (D_2O solvent, 10 mM HEPES buffer, 0.5 M NaCl, pH = 7.40) as a function of increasing concentration (%v/v) of TFE recorded at 298 K.

(b) Set II: MLT without buffer in various compositions of TFE: Figure 5.5 represents the CD spectra of set-II MLT samples as a function of TFE composition. For these samples, the pH has been found to be equal to 2.75±0.10. In general a dip at 202 nm is representative of random coils in a CD spectrum. In figure 5.5, a minimum CD angle at 202 nm is observed for MLT in 100% D_2O (*ie*, 0% TFE), indicating a random coil MLT with absence of any significant secondary structure in the polypeptide [Jasanoff and Alan, 1994]. On the other hand, the addition of TFE changes the random coil CD spectrum of MLT to the characteristic α-helical curve. The amphiphilic nature of TFE is responsible for its structure inducing property, *i.e.* inducing and stabilizing α-helicity. The characteristic α-helical negative dips at 207 nm and 221 nm arise because of induced α-helicity in MLT structure with increasing TFE concentration. α-helical content of a peptide/protein can be monitored by measuring the intensity of the CD peak at 221 nm: higher peak intensity at this wavelength reflects more helicity. As per the literature, if there is no local unfolding, the measured helicity (negative CD angle) will be directly proportional to the amount of tetramer formed [Wilcox and Eisenberg, 1992].

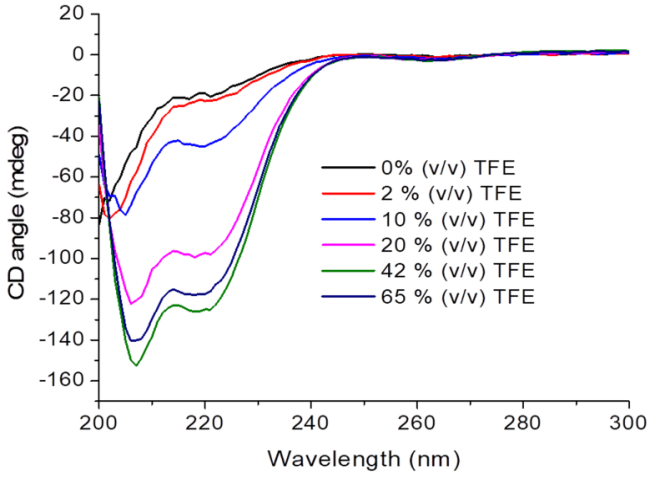

Figure 5.5: CD spectra of MLT in set-II (D_2O solvent, pH=2.75) as a function of increasing concentration (% v/v) of TFE recorder at 298 K.

From the CD curves in figure 5.5, maximum helicity can be seen at 42% TFE. Therefore, it can be said that at 42% TFE, considerable amount of MLT might have aggregated into tetramer form. The decrease in helicity for 65% TFE, on the other hand, can be understood by noting that the relatively high concentration of TFE in water is capable of disrupting the hydrophobic interactions, resulting in denaturation of the tertiary and secondary structures [Cammers-goodwin et al., 1996]. It can, therefore, be concluded that low concentration of TFE induces and stabilizes α-helicity, while with higher concentration of TFE, the mechanism of stabilization is different and less dramatic in nature. The structural transitions for MLT (at a fixed concentration) in presence of various compositions of TFE: D_2O solvent system showed that the solvent plays an important role in defining protein / peptide structural integrity. It can be envisaged that the dynamics of TFE molecules around aqueous MLT plays an important role in bringing about the structural changes in MLT polypeptide chain. Therefore, probing the alterations of TFE behaviour in presence of such structural transition would provide an alternative avenue to address MLT solution dynamics. A point to be noted here is that a series of CD measurements performed for set-II samples with a larger range of TFE: D_2O compositions ranging from 2–95% of TFE revealed that MLT behaves in a similar way above 42% TFE for all higher concentrations of TFE used. The corresponding CD spectrum is shown as figure 5.6 where coloured codings from 2% to 95% represent the % (v/v) compositions of TFE wrt D_2O. It can be seen that the negative CD angle initially increases from 2% to 42% (v/v) TFE concentration and after 42%, always a decrease in MLT CD angle was seen from 50% upto 80%. Therefore, 65% (v/v) TFE: D_2O is chosen as a representative higher concentration of TFE (beyond 42% (v/v) TFE solvent composition) for analysing the decreasing trend of CD angles in the set-II samples. A thorough search of the literature confirms that MLT transitions studied at the five reported concentrations (2%, 10%, 20%, 42%, 65%) are suitable to indicate that the TFE-induced structural transformation is best described as a three-state equilibrium, Native (N)↔Intermediate (I)↔Helical (H), with the (I) state being most populated around 10–20% of TFE [Kumar et al., 2003; Kuwata et al., 1998; Mendieta et al., 1999].

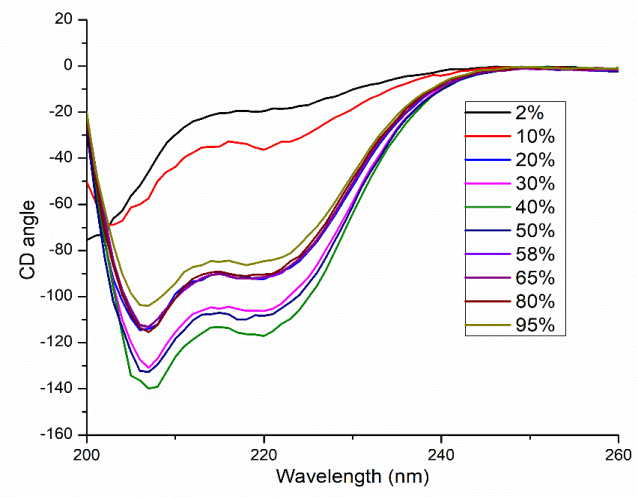

Figure 5.6: CD spectra of MLT in TFE: D_2O solvent (set-II) as a function of increasing (% v/v) of TFE composition (pH=2.75) at T=298 K

(ii) NMR measurements:

In order to confirm the CD observations related to MLT transitions in presence of TFE, ^1H NMR of MLT is recorded for both set-I and set-II samples at 500 MHz. ^1H NMR spectra of MLT protons (aromatic tryptophan peaks and aliphatic peaks) in pure D_2O (figure 5.7) and with increasing concentration of TFE in set-I (pH 7.4) and in set-II (pH 2.8) solutions are shown as figure 5.8 (a & b) respectively. The monomer and tetramer form of MLT at pH 2.8 and pH 7.4 respectively is verified from the corresponding ^1H NMR spectra following the work of Y. Miuara et al., [Miura, 2012, 2016], J. Lauterwein [Lauterwein et al., 1980] and L. R. Brown (1980) [Brown et al., 1980]. MLT NMR peaks in pure D_2O (figure 5.7) are found consistent with the spectrum of the random coil form reported in the literature. Addition of TFE resulted in downfield shift of the NMR peaks, with considerable line broadening compared to the NMR peaks of MLT in 0% TFE. This observation is consistent with the characteristic α-helical structure of MLT as represented in figure 5.8.

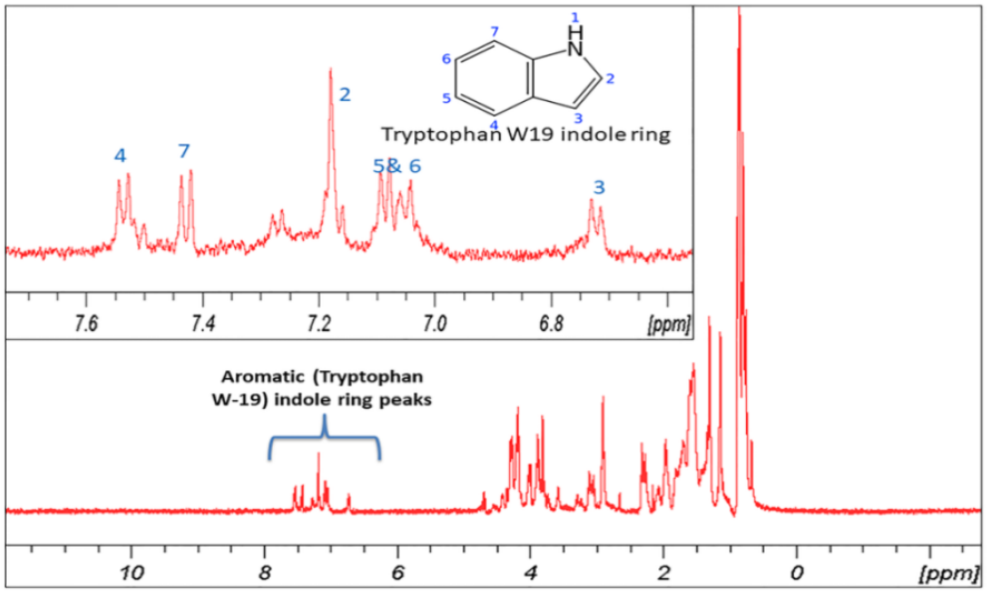

Figure 5.7: Water suppressed 500 MHz ^1H NMR spectrum of 1 mM MLT in 100% D_2O (0% TFE) at 298 K. Inset shows the aromatic tryptophans' indole (W-19) proton peaks.

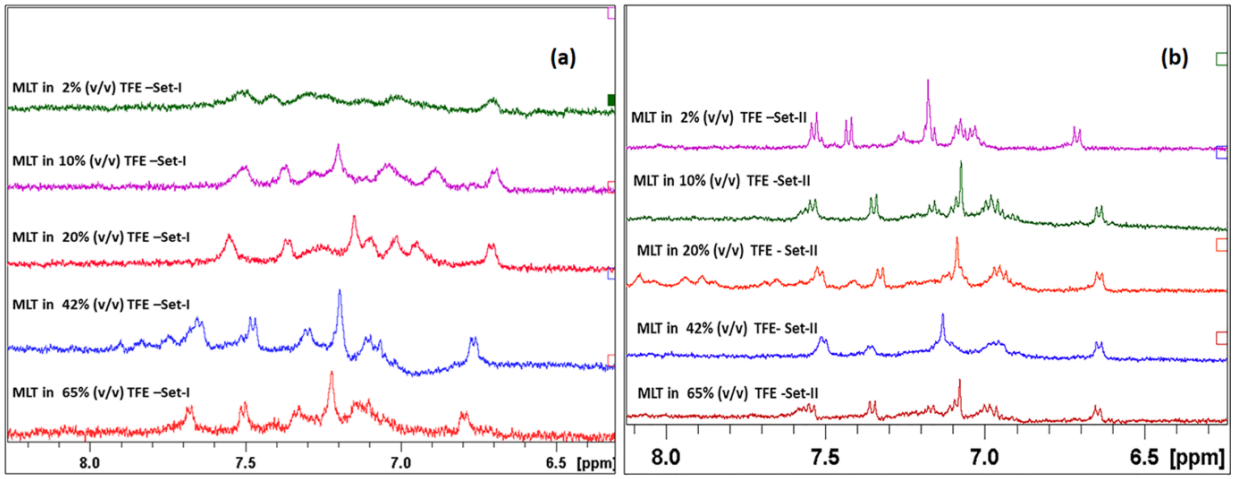

Figure 5.8: 500 MHz ^{1}H NMR spectrum of 1 mM MLT as function of TFE compositions for (a) set–I (D_2O solvent, 10 mM HEPES buffer, 0.5 M NaCl, pH= 7.40) and set–II (D_2O, pH=2.75) samples recorded at 298 K.

In case of set-I MLT samples, MLT is predominantly helical, exhibiting broad, low intensity peaks in the NMR spectrum assigned to the tetramer form of MLT [Fioroni et al., 2002] given in figure 5.8 (a). With increasing concentration of TFE, the peaks get narrower, corresponding to the monomeric form of MLT. On the other hand, for set-II samples, with increasing concentration of TFE the NMR peak width increases along with 'loss' of loss of fine structure or apparent peak multiplicity; this can be related to oligomerization of MLT (figure 5.8 (b)). These sets of measurements using ^{1}H NMR and CD spectroscopy clearly indicated the influence of TFE concentration on the monomer to self-aggregate/tetramer transition, prompting interest in analysing the effect of TFE as a co-solvent on the transition process. Therefore, the present study mainly focuses to highlight the solvation dynamics of TFE around MLT as a function of solvent composition, at which MLT exists in different conformational states. In the following this issue has been addressed by employing low field spin-lattice relaxation and ODNP for detecting molecular dynamics in solution. The particular analysis allows to show-case applicability of low field ^{19}F spin-lattice relaxation measurements in conjunction with low field ODNP revealing solute-solvent interaction.

(a) Relaxation Measurements: NMR relaxometry enables detection of alterations in the dynamic behaviour of solvent that are caused due to the presence of solute molecules [Bryant, 1978; Kumar et al., 2003]. There is a considerable body of literature on the application of relaxometry to probe dynamics of water/solvent around proteins [Kemple et al., 1997; Kumar et al., 2003; Sabadini et al., 2008; Yuan et al., 1996]. The effect of molecular interaction between solute and solvent can be investigated by probing relaxation of any of the partners.

^{19}F Relaxation measurements at 13.7 MHz (0.34 T)

Longitudinal relaxation rate (R_1) of ^{19}F of TFE reflects the dynamical behaviour of TFE molecules around MLT. For the present case, low field ^{19}F NMR relaxation analysis of TFE has been employed in order to investigate the solvation dynamics of the MLT–TFE system. This approach results in specific advantages over the corresponding high field ^{19}F relaxation data acquired for the same system that are found insufficient to reveal any dynamical information for the aforementioned solvent-solute interaction. ^{19}F and ^{1}H longitudinal relaxation rate (R_1) for TFE (–CF_3 & –CH_2) were measured for set-I and set-II samples at 11.7 T. Figure 5.9 (a & b) represents the plot of ^{19}F and ^{1}H R_1 against concentration of TFE. In both cases of set-I and set-II, the comparative changes (in presence and absence of MLT) in ^{1}H R_1 (–CH_2) values are higher than that of ^{19}F R_1 values (–CF_3). A rough estimation shows that for 2% (v/v) TFE the comparative

change in ^{19}F R_1 for both sets was only *ca.* 2% while for the same concentration the change in ^{1}H R_1 was found to be *ca.* 13%. This could be attributed to the fact that proton R_1 values depend largely on dipolar interaction. In addition to these measurements, ^{19}F R_2 was measured for solvent TFE ($-CF_3$) for both the sets and the relaxation rate R_2 is plotted against concentration of TFE in figure 5.10**.** Unlike ^{19}F R_1, a significant variation in ^{19}F R_2 was observed for TFE samples with and without MLT for both the sets. This observation matches well with the literature where it is mentioned that ^{19}F R_2 is more sensitive towards molecular interaction compared to ^{19}F R_1. Such behaviour of ^{19}F relaxation could be attributed to the effect of CSA as a pronounced relaxation mechanism in solution. This effect of CSA becomes more prominent especially at higher magnetic fields [Gerig, 1997].

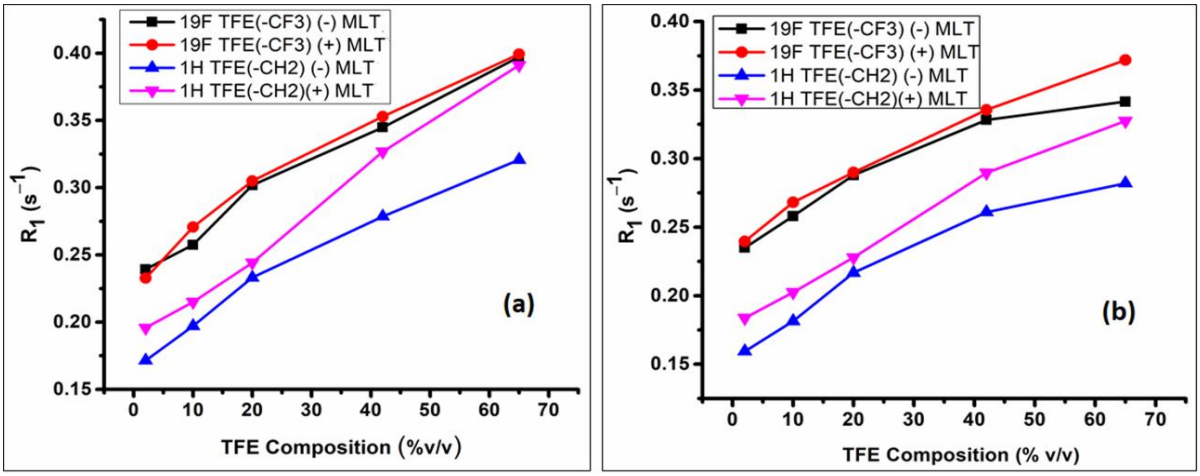

Figure 5.9: Plot of measured ^{19}F ($-CF_3$) and ^{1}H ($-CH_2$) R_1 of TFE at 500 MHz in absence and presence of MLT as a function of TFE composition in (a) set–I (D_2O solvent, 10 mM HEPES buffer, 0.5 M NaCl, pH= 7.40) (b) set–II (D_2O solvent, pH= 2.75) samples at T=298 K.

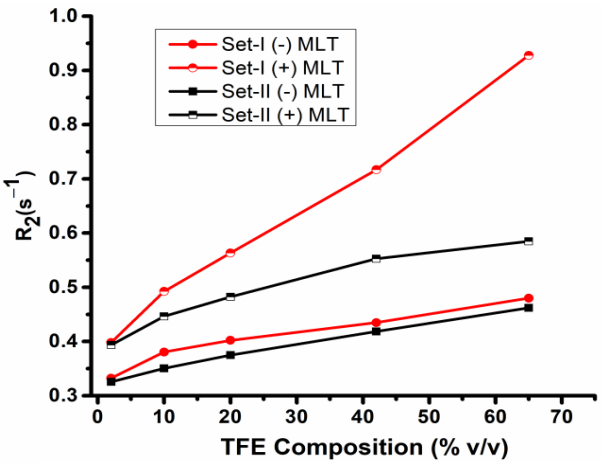

Figure 5.10: Plot of measured ^{19}F ($-CF_3$) R_2 of TFE various compositions for set–I (D_2O solvent, 10 mM HEPES buffer, 0.5 M NaCl, pH=7.40) and set–II (D_2O solvent, pH=2.75) in absence (–) and presence (+) of MLT at 500 MHz measured at 298 K.

R_2 exhibited higher changes, e.g., a 17.3% change was observed (without and with MLT) for 2% (v/v) TFE in both set-I and set-II samples. In absence of MLT, the change in R_2 values of

TFE with increasing TFE concentration for both the set of solutions is almost identical indicating that the pH and solution conditions have negligible effect on the TFE relaxation rates. However, in presence of MLT, the R_2 value of TFE showed a striking increase from 17% to 48% with an increase of TFE composition from 2% (v/v) to 65% (v/v) in set-I, while for set-II the increase was of a moderate amount *i.e.,* 17% to 22% only. This clearly suggests that the dynamical behaviour of TFE is different in both sets in presence of MLT. The decrease in relaxation rates *i.e.* ^{1}H R_1 and ^{19}F R_2 in presence of MLT compared to TFE samples without MLT undoubtedly points out that TFE is interacting with MLT. However, quantification of molecular motion from these set of relaxation data becomes cumbersome due to contribution of CSA relaxation mechanism at high magnetic field [Gerig, 1997]. Moreover, the changes observed in case of ^{19}F TFE diffusion coefficient in absence and presence of MLT are less striking, and discourage further analysis (data not shown).

The ^{19}F R_1 is measured for both set-I (D_2O solvent, 10 mM HEPES buffer, 0.5 M NaCl, pH=7.40) and set-II (D_2O solvent, pH=2.75). The low field relaxation study for ^{19}F reduces the effect of CSA in relaxation measurements: in the present case by three orders of magnitude at 0.34 T as compared to 11.76 T, since the corresponding relaxation rate is proportional to the square of the Zeeman field (B_0). Moreover, on the model of intramolecular relaxation due to molecular tumbling, this approach simplifies the inference of the rotational correlation time of the solvent as it fulfils the extreme narrowing condition [$(\omega_F+\omega_H)^2\tau_c^2<<1$]) up to a rotational correlation time that is as long as *ca.* 552 ps. One may anticipate that the longitudinal relaxation rate of ^{19}F liquid TFE reflects principally the intramolecular dipolar interactions which include homonuclear (^{19}F–^{19}F) and heteronuclear (^{1}H–^{19}F) dipolar interactions, more so at low TFE concentrations [Gerig, 1997; Kumar et al., 2003; Lambert and Simpson, 1985]. In the absence of interference or cross correlation between homo– and heteronuclear dipolar interactions, the ^{19}F relaxation rate under extreme narrowing conditions may be expressed in SI units as [Abragam, 1961; Solomon, 1955]:

$$R_{F_i} = R_{F_iF_{j\neq i}} + R_{F_iH} = \left(\frac{\mu_0}{4\pi}\right)^2 \gamma_F^2 \hbar^2 \tau_c \left[\frac{3}{2}\gamma_F^2\left(\sum_j \frac{1}{r_{F_i-F_{j\neq i}}^6}\right) + \gamma_H^2\left(\sum_k \frac{1}{r_{F_i-H_k}^6}\right)\right] \quad ....(5.1)$$

Here, μ_0 and γ_i are the permeability of free space and the gyromagnetic ratio of the *i*-th spin, respectively, while *r*: inter-spin distance. In writing equation 5.1, the extreme narrowing limit [$(\omega_F+\omega_H)^2\tau_c^2 \leq 0.01$] has been applied to the well-known standard expression for relaxation arising from fluctuating dipolar interactions between spins, and the motional spectral density function $J(\omega_i,\tau_c)$ relevant for intramolecular relaxation mediated by random isotropic molecular tumbling [Abragam, 1961] is employed as expressed in equation 5.2.

$$J(\omega_i,\tau_c) = C\left(\frac{\tau_c}{1+\omega_i^2\tau_c^2}\right) \quad .....(5.2)$$, here C is the fluctuating field constant

The preceding discussion on ^{19}F relaxation invoked several approximations in writing equation 5.1: i) ^{19}F nuclei in TFE are relaxed entirely by the dipole-dipole mechanism [Kumar et al., 2003; Radnai, et al., 1989]; ii) any contributions from the shielding anisotropy has been neglected at the low magnetic field as discussed earlier; iii) effect of spin-rotation has been omitted considering the fact that the contribution of this mechanism to R_1 is significant only at elevated temperatures (48 and 66°C) as demonstrated by an earlier ^{19}F relaxation study of neat TFE [Lambert and Simpson, 1985]; iv) negligible contribution of the intermolecular dipole coupling between ^{19}F of TFE and ^{1}H of water as well as intramolecular interaction between ^{19}F and ^{1}H of –OH group of TFE due to longer spatial separation [Kumar et al., 2003]; v) the cross-correlation effects in the ^{19}F three-spin system of the CF_3 group have been ignored since theoretical analysis of the analogous CH_3 system indicates that such effects are very small [Lee and Hwang, 1990]. In summary, for the present case, as the relaxation measurements are carried out at low field and room temperature (*ca.* 26 °C) contributions of CSA and spin-rotation

mechanism to R_1 would not be significant. Only the dipole interactions of ^{19}F with the other two F atoms of CF_3, as well as with the two protons in the adjacent CH_2 group have been considered as the active relaxation mechanisms.

The ^{19}F R_{1F} measurements of TFE are repeated three times for each sample to extract the standard deviation in the final reported relaxation rates. From the R_{1F} values, the rotational correlation time (τ_c) of TFE for various compositions of TFE has been inferred. τ_c of TFE in the absence and in the presence of MLT at different compositions of TFE: D_2O are calculated using Eq. (5.1) and is reported in table 5.2. Two interatomic ^{19}F–^{19}F distances (2.17 Å, 2.18 Å) and two interatomic ^{1}H–^{19}F distances (2.64 Å, 3.29 Å) *[Ref: Automated Topology Builder (ATB) and Repository. http://atb.uq.edu.au/viewer.py?molid=363882]* of TFE are used for the calculation of rotational correlation times and values are reported in table 5.2.

Table 5.2: Extracted molecular rotational correlation time (τ_c) from T_1 values (T_1=1/R_1) measured at 13.7 MHz for TFE in absence and presence of MLT for set-I (D_2O solvent, 10 mM HEPES buffer, 0.5 M NaCl, pH=7.40) and set-II (D_2O solvent , pH=2.75) samples.

Sample	Set-I (pH=7.40)		Set-II (pH=2.75)	
	R_1 (s^{-1})	τ_c (ps)*	R_1 (s^{-1})	τ_c (ps)*
2% (v/v) TFE in D_2O	---------	---------	0.178±0.007	12.26±0.48
1 mM MLT in 2% (v/v) TFE in D_2O	---------	---------	0.212±0.009	14.64±0.61
10% (v/v) TFE in D_2O	0.255±0.009	17.59±0.61	0.216±0.008	14.86±0.55
1 mM MLT in 10% (v/v) TFE in D_2O	0.307±0.004	21.12±0.27	0.239±0.009	16.48±0.61
20% (v/v) TFE in D_2O	0.299±0.005	20.56±0.34	0.222±0.005	15.26±0.34
1 mM MLT in 20% (v/v) TFE in D_2O	0.325±0.003	22.36±0.20	0.243±0.004	16.74±0.27
42% (v/v) TFE in D_2O	0.354±0.006	24.37±0.41	0.303±0.003	20.85±0.20
1 mM MLT in 42% (v/v) TFE in D_2O	0.375±0.007	25.84±0.48	0.320±0.004	22.06±0.27
65% (v/v) TFE in D_2O	0.410±0.005	28.25±0.34	0.351±0.004	24.14±0.27
1 mM MLT in 65% (v/v) TFE in D_2O	0.431±0.005	29.64±0.34	0.398±0.005	27.42±0.34

(*propagated errors in their ratios are reported in table 5.3)

It has been noted that in case of small rigid molecule undergoing isotropic motion, the assumption of single correlation time involved in modulating the hetero- and homo-nuclear intra-molecular dipole-dipole interactions is valid [Becker, 2000; Gerig, 1997; Kumar et al., 2003]. It is to be pointed out that in the system with MLT, the longitudinal relaxation rate of TFE would be the weighted average of bulk TFE and TFE in the solvation sphere of MLT [Becker, 2000; Gerig, 1997]. Mono-exponential decay for ^{19}F R_1 (R_{1F}) has been obtained in all the cases. This observation of mono-exponential magnetization decay further confirms that the relaxation is dynamically averaged between two environments namely bulk TFE and TFE bound to MLT [Beek et al., 1991]. In presence of MLT, the experimentally measured ^{19}F TFE relaxation rates (R_1) exhibit enhancements for both the sets clearly reflecting the effect of the bound TFE on the R_1. Consequently, at a fixed composition of TFE, it has been observed that in presence of MLT the rotational correlation time of TFE (τ_c^{MLT}) is longer compared to the correlation time of TFE in its absence (τ_c^{free}). This strengthens the understanding that in presence of MLT, TFE interacts with MLT and exists in an ordered solvation region of MLT. Moreover, it is also reported in the literature that the density of TFE around the MLT is considerably higher as compared to the bulk phase. Therefore, the rotational correlation time of TFE in the presence of MLT may be considered to reflect predominantly the correlation time of TFE in the solvation sphere of the

MLT molecules. To take into account the possible effect of alteration of viscosity (due to increasing concentration of TFE and presence of MLT) on the measured TFE relaxation rates, the viscosity of all the samples of set-I (pH=7.40) and set-II (pH=2.75) have also been measured and reported in figure 5.11. The viscosity of the solution increases with increasing composition of TFE; however, addition of 1 mM MLT to the samples of same concentrations did not bring any significant changes to the viscosity of the samples. Hence, it can be stated with confidence that at a particular composition of TFE the enhancement in TFE relaxation rate/correlation time is solely due to interaction of TFE with MLT.

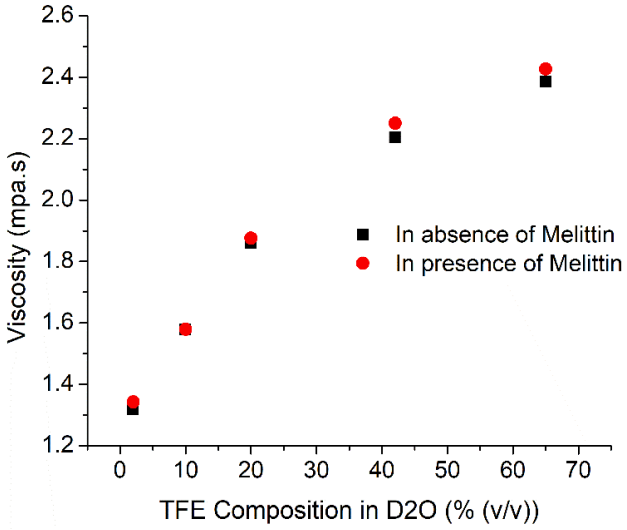

Figure 5.11: Plot of measured viscosity for TFE: D_2O solutions in absence and presence of MLT (set-II, D_2O solvent, pH= 2.75) as a function of increasing % (v/v) TFE concentration.

In order to understand the conformational change of MLT with increasing concentration of TFE in the system, the ratios of correlation times ($\tau_c^{MLT}/\tau_c^{free}$) have been analysed in the presence and absence of MLT for different compositions of TFE. Figure 5.12 and table 5.3 demonstrate the variation of ($\tau_c^{MLT}/\tau_c^{free}$) as a function of TFE composition. A number of interesting facts are revealed on analysing the trend of variation of the ratio with changing TFE composition: **i)** In the case of set-I (pH=7.40) samples, the ratio ($\tau_c^{MLT}/\tau_c^{free}$) decreases continuously with increasing concentration of TFE; **ii)** In the case of set-II (pH=2.75) samples, a similar decreasing trend for the ratio ($\tau_c^{MLT}/\tau_c^{free}$) is observed up to 42% (v/v) TFE: D_2O solvent, while at 65% (v/v) TFE: D_2O, the ratio increases; **iii)** both the sets exhibit a similar trend of the ratio of correlation time in 20% to 42% (v/v) TFE composition range; **iv)** significantly higher changes in the ratios are seen for lower concentration of TFE in the solution, more specifically between 10–20% concentration range. It is to be mentioned here that the ratio of correlation times ensures removal of the effect of viscosity variation as a function of TFE concentration on the correlation times. Also, as discussed earlier (figure 5.11), the addition of MLT do not bring any significant changes in solution viscosity for lower TFE concentrations (upto 30%). Even at the higher TFE concentrations (42% and 65% (v/v)), the change in viscosity of the samples are only 2% and 1.73% respectively. Therefore, the effect of viscosity can be considered to be negligible.

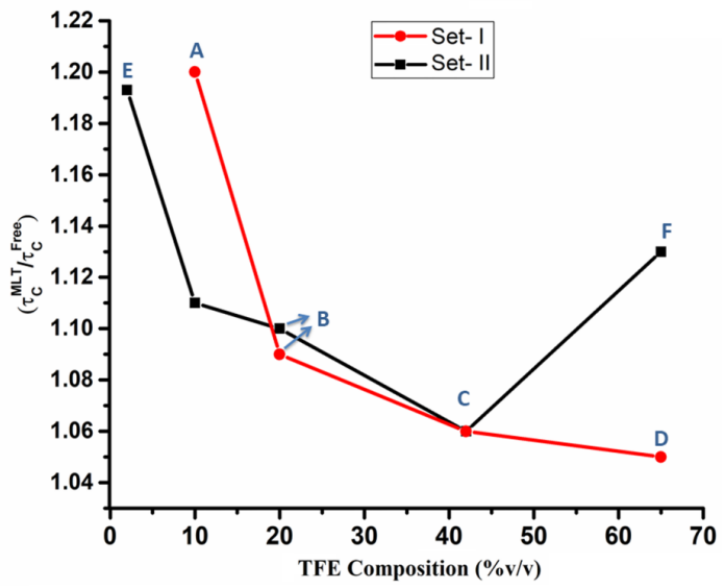

Figure 5.12: Plot of ratio of correlation times ($\tau_c^{MLT}/\tau_c^{free}$) for various compositions of TFE for set-I (D_2O solvent, 10 mM HEPES buffer, 0.5M NaCl, pH=7.4) and set-II (D_2O solvent, pH=2.75) samples). Set-I (A: Tetrameric/Self aggregated state, D: Monomeric open helical state). Set-II (E: Monomeric random coiled, F: Dense open helical state). Set-I and set-II (B and C: Mixed helical monomeric and aggregated state).

Table 5.3: Ratio of correlation times ($\tau_c^{MLT}/\tau_c,^{free}$) with various compositions of TFE for set-I (D_2O solvent, 10 mM HEPES buffer, 0.5 M NaCl, pH= 7.40) and set-II (D_2O solvent, pH= 2.75) samples at low field (0.34T).

Sample	Correlation time ratio (Set-I)	Correlation Time ratio (Set-II)
2% (v/v) TFE in D_2O	---------	1.194±0.097
10% (v/v) TFE in D_2O	1.204±0.058	1.109±0.082
20% (v/v) TFE in D_2O	1.087±0.028	1.097±0.042
42% (v/v) TFE in D_2O	1.059±0.037	1.058±0.023
65% (v/v) TFE in D_2O	1.051±0.025	1.136±0.027

The observations made in the present case can be explained as follows: **i)** the trend of decreasing ratio of correlation time of TFE ($\tau_c^{MLT}/\tau_c^{free}$) with increasing concentration of TFE in case of set-I indicate possible depletion of TFE molecules from solvation sphere of MLT. Therefore, addition of TFE in set-I samples induces the gradual conformational change of self-aggregated/ tetrameric MLT to monomeric open helical MLT. It can be inferred that in monomeric form of MLT, a greater number of TFE molecules will be in the bulk phase compared to the TFE in aggregated conformation of MLT [Othon et al., 2009; Roccatano et al., 2002]. As a result, the ratio of motional correlation times of TFE is closer to 1 in case of monomeric MLT as compared to its aggregated conformation. These observations are found to be consistent with the CD results mentioned in figure 5.4 which showed tetramer to monomer transition for MLT set-I samples; **ii)** the decrease in the ratio of motional correlation times from 10% to 42% in case of set-II samples is representative of TFE interaction with MLT however, it should be pointed out that in case of set-II samples the initial conformation of MLT is monomeric random coil in nature as confirmed from the CD spectrum. Hence, striking difference in the ratio of correlation times at lower (*ca.* 10%) and at higher (*ca.* 65%) % (v/v) TFE concentration could be identified while comparing set-II samples with that of set-I samples. At 10% (v/v) TFE concentration, the extracted correlation time ratio is found significantly lower in

case of set-II compared to set-I. This is consistent with the remark that TFE density around monomeric MLT is lower compared to the TFE density when MLT is in aggregated form. Furthermore, increase of the ratio ($\tau_c^{MLT}/\tau_c^{free}$) is observed in case of set-II on moving towards higher concentration of TFE (65% (v/v) TFE: D_2O). This is probably due to the fact that at this concentration, TFE density around MLT sphere increases and prevents the aggregation of MLT in set-II samples; **iii)** the similar nature of the ratio of correlation time in set-I and set-II samples in the concentration range of 20–42% suggested that TFE density around MLT is nearly same in both the sets in this concentration range. One may anticipate that MLT might be transiting through similar conformational intermediate state (*i.e.* mixed monomeric and aggregated state) in both the pH conditions. As it is understood from the analysis of CD spectra that in case of set-I, MLT is showing structural transition from folded helical (aggregated) state to open helical state whereas in set-II, it is moving from random coiled to dense open helical state; **iv)** the higher changes in the ratios observed for lower concentration of TFE compared to high TFE concentration matched well with the literature. It has been reported that TFE undergoes molecular crowding (evidenced from the observation that TFE R_1 in absence of MLT increases with increasing TFE compositions) in 10–30% concentration range and brings the maximum conformational change of macromolecular systems in this range [Culik et al., 2014].

The present set of outcomes can be completely correlated with previous literature on the effect of TFE on macromolecular conformational changes. It has been reported that at low TFE percentages, folding/aggregation tendency of macromolecules is increased due to stabilization of native hydrogen-bonding groups, whereas at higher percentages of TFE, folding rates are decreased in a similar manner as it is found in case of denaturants due to TFE's interaction with buried residues. In the current analysis TFE always acted as a denaturant whether present in low or high concentration in case of set-I samples, while in case of set-II samples it induces higher order structure at low concentration whereas acted as a denaturant only at a higher concentration. It must be emphasized here that the current analysis proves that low field relaxation experiments can provide powerful insights on conformational changes of MLT, highlighting the solvent dynamics.

(b) Overhauser Dynamic Nuclear Polarization (ODNP) Measurements:

In order to find additional support for the relaxation studies at moderately low field (0.34 T), steady state ODNP experiments are also performed at the same field for all the compositions of the MLT–TFE system in the presence of TEMPOL free radical (5 mM). A comparative analysis of ^{19}F ODNP of TFE is done to investigate the change in solvation dynamics of TFE in presence and in absence of MLT.

Here, the ODNP hyperpolarization is generated on saturating the EPR transitions of added TEMPOL by continuously irradiating microwaves, followed by the acquisition of the NMR signal employing a 90° radiofrequency pulse [Abragam, 1953; Bates, 1993]. The expression of steady state ODNP enhancement factor A in terms of the EPR saturation parameter (s) of the added free radical, the substrate nuclear spin relaxation leakage factor (f) and the ODNP coupling parameter (ξ) is given in equation 2.26 (details of ODNP parameters are given in Chapter 2, section-2.6.2). The ODNP coupling parameter ξ, which is the ratio of the electronτnuclear cross and auto relaxation rates, plays a vital role in characterizing the fluctuating interaction between the electron and nuclear spins. This interaction, which in general could be dipolar or scalar in origin, or of mixed nature, is modulated by molecular motions that may be characterized by the radical–substrate molecule correlation time, reflecting the motional dynamics in solution-state [Borah and Bates, 1981a, 1981b]. It is important to note that ^{19}F ODNP shows mixed scalar and dipolar interactions [George and Chandrakumar, 2014], which are not separable based on measurements at a single field at a fixed temperature. Therefore, extraction of the motional correlation time from the ^{19}F coupling parameter is not straightforward. However, the observed ^{19}F ODNP enhancement of TFE at 0.34 T in the present system indicates

that the dipolar interaction between ^{19}F and the unpaired electron of TEMPOL dominates, which results in negative enhancements. If it may be considered that scalar cross relaxation by the radical is essentially unaffected in the presence of MLT, it would appear reasonable to qualitatively analyse the variation in ^{19}F ξ at 0.34 T in presence and absence of MLT in terms of the variation in dipolar interaction, at fixed radical concentration. Tables 5.4 and 5.5 summarize the relevant ODNP parameters including the ^{19}F ξ value for all the compositions of the MLT–TFE system in set-I and set-II respectively, in the presence of 5 mM TEMPOL.

Table 5.4: Relevant ^{19}F ODNP parameters at various compositions of TFE with respect to D_2O for set-I (D_2O solvent, pH=7.4, 10 mM HEPES buffer, 0.5 M NaCl) samples. *A*= enhancement factor

Set-I in 5 mM TEMPOL	*A*	Saturation factor	leakage	Coupling parameter
10% (v/v) TFE	−42.7	0.77	0.91	0.086
10% (v/v) TFE + 1 mM MLT	−24.3	0.77	0.81	0.055
20% (v/v) TFE	−36.7	0.77	0.89	0.076
20% TFE (v/v) + 1 mM MLT	−26.7	0.79	0.82	0.058
42% TFE (v/v)	−25.1	0.7	0.89	0.057
42% TFE (v/v) + 1 mM MLT	−20.2	0.74	0.82	0.047
65 % TFE (v/v)	−23.5	0.71	0.88	0.054
65 % TFE (v/v) + 1 mM MLT	−19.3	0.7	0.78	0.05

Table 5.5: Relevant ^{19}F ODNP parameters at various composition of TFE with respect to D_2O for set-II (D_2O solvent, pH=2.75) samples.

SetII in 5 mM TEMPOL	*A*	Saturation factor	leakage	Coupling parameter
2% (v/v) TFE	−38.2	0.7	0.85	0.09
2% (v/v) TFE + 1 mM MLT	−27	0.73	0.83	0.064
10% (v/v) TFE	−44.7	0.78	0.85	0.09
10% (v/v) TFE + 1 mM MLT	−35.3	0.79	0.85	0.075
20% (v/v) TFE	−35.1	0.79	0.87	0.072
20% TFE (v/v) + 1 mM MLT	−29.7	0.77	0.86	0.062
42% TFE (v/v)	−27.3	0.72	0.83	0.065
42% TFE (v/v) + 1 mM MLT	−28	0.72	0.87	0.063
65 % TFE (v/v)	−29.3	0.67	0.83	0.074
65 % TFE (v/v) + 1 mM MLT	−25.6	0.69	0.86	0.063

In general, at a particular composition of TFE, a decrease in ξ is observed when MLT is present in the system, suggesting an increase in the electron-nuclear correlation time [Abragam, 1953; Armstrong and Han, 2009; Bates, 1993; Carver and Slichter, 1953; Hausser and Stehlik, 1968; Hubbard, 1966; Overhauser, 1953] . It supports the fact that TFE in the solvation sphere of MLT remains in an "ordered" state compared to TFE in bulk phase (*ie*, system in absence of MLT), resulting in longer radical-TFE translational correlation times.

Moreover, in order to understand the effect of increasing concentration of TFE on the conformation of MLT, the ratio of coupling parameters has been analysed in presence and absence of MLT (ξ^{MLT}/ξ^{Free}) for set-I and II at different concentrations of TFE (figure 5.13).

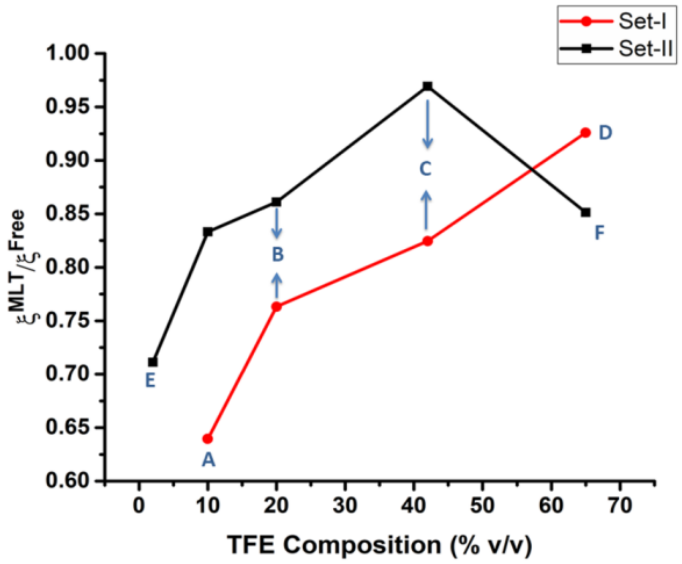

Figure 5.13: Plot of (ξ_{MLT}/ξ_{Free}) obtained from ODNP experiments as a function of various composition of TFE for set-I (D_2O solvent, 10 mM HEPES buffer, 0.5 M NaCl, pH=7.4) and set-II (D_2O solvent, pH=2.75). Set-I (A: Tetrameric/ Self aggregated state, D: Monomeric open helical state). Set-II (E: Monomeric random coiled, F: Dense open helical state). Set-I and set-II (B and C: Mixed helical monomeric and aggregated state)

In analogy with the considerations in respect of the low field relaxation data (*vide supra*), it is important to note here that comparison of this ratio of coupling parameters at different TFE compositions removes the effect of viscosity variation with TFE concentration. With increasing concentration of TFE for set-I, an increase in (ξ^{MLT}/ξ^{Free}) is observed, that tends to 1. This reflects reduced changes in the correlation time of TFE between bulk and 'MLT' phases at higher concentrations of TFE. In turn, this reflects a transition of the aggregated/ tetrameric state to monomeric state. Similarly, ODNP experiments are performed on MLT–TFE (set-II) systems in presence of 5 mM TEMPOL. In the case of set-II (table 5.5), the trends in (ξ^{MLT}/ξ^{Free}) are similar up to 42% (v/v) of TFE; the ratio reduces at higher concentrations of TFE. The body of observations and inferences discussed based on ODNP above matches satisfactorily with those from ^{19}F low field relaxation studies, establishing steady state ^{19}F ODNP as a complementary method to probe such conformational changes of oligopeptides. Figure 5.14 summarizes the overall behaviour of molecular system investigated in the current study in a pictorial form based on the previous literature support and obtained experimental data. It can be further elaborated as follows:

i) 0–2% (v/v) TFE:D_2O at pH 7.40 stabilizes tetrameric or aggregated form (A).
ii) 0–2% (v/v) TFE:D_2O at pH 2.75 prefers random coiled form (E).
iii) 10–42% (v/v) TFE:D_2O at both pH 7.40 & 2.75 retains an intermediate state of MLT (B & C).
iv) For 65% and above, monomeric open helix (D) exist at pH 7.4 while dense open–helix (F) exist at pH=2.75.

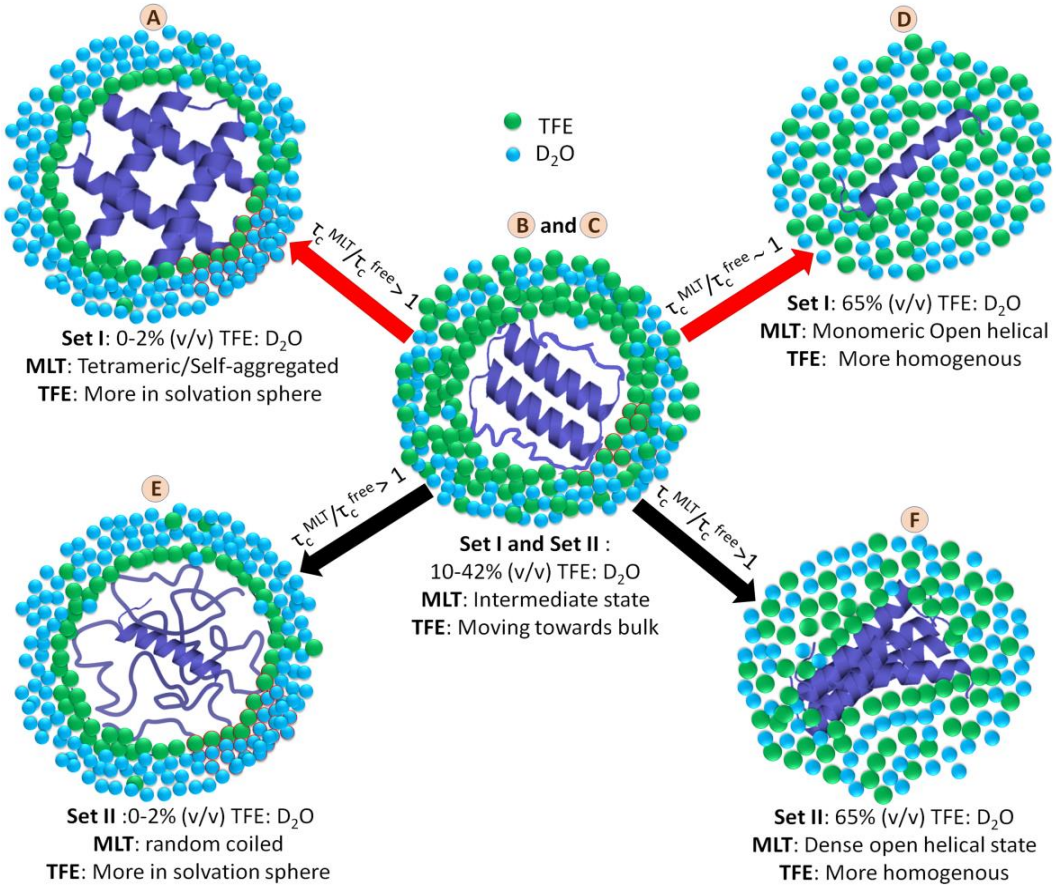

Figure 5.14: Graphical representation summarizing the various possible conformational forms of MLT and the respective TFE solvent dynamics around these conformations.

5.3.2 Part II: Preferential solvation of carbohydrates in TFE: D_2O mixture

Figure 5.15 shows a representative stack plot of ^1H NMR spectra of carbohydrate β-CD in TFE: D_2O co-solvent mixture. It is clearly seen that in the presence of TFE, the peaks of β-CD get overlapped with the TFE solvent peak. This is a common trend of carbohydrates where overlapped ^1H spectra, especially in the region of solvent are observed. It can be seen from the figure 5.15 that in the presence of TFE, all the peaks of β-CD experienced a drift in chemical shifts along with significant amount of line-broadening. This is representative of (a) the change in chemical environment of β-CD due to interaction with TFE, or (b) change in the viscosity of the solution. β-CD inner protons (H_3 and H_5) show upfield shifts while all the outer protons (H_2, H_1, H_4) have shifted downfield. A close inspection of the figure 5.15 also reveals that the changes in chemical shifts experienced by inner protons (H_3 and H_5) are comparatively greater in magnitude with respect to that of the external protons of β-CD. It could be a result of complexation between TFE and β-CD inner protons consequent to the TFE solvation phenomenon. A wider picture of solvation happening in the β-CD solution can be obtained by monitoring the solvent peaks more effectively since a single solvent peak is observed both in the case of ^2H for D_2O and in the case of ^{19}F for TFE mitigating the spectral complexities observed in the carbohydrate spectrum.

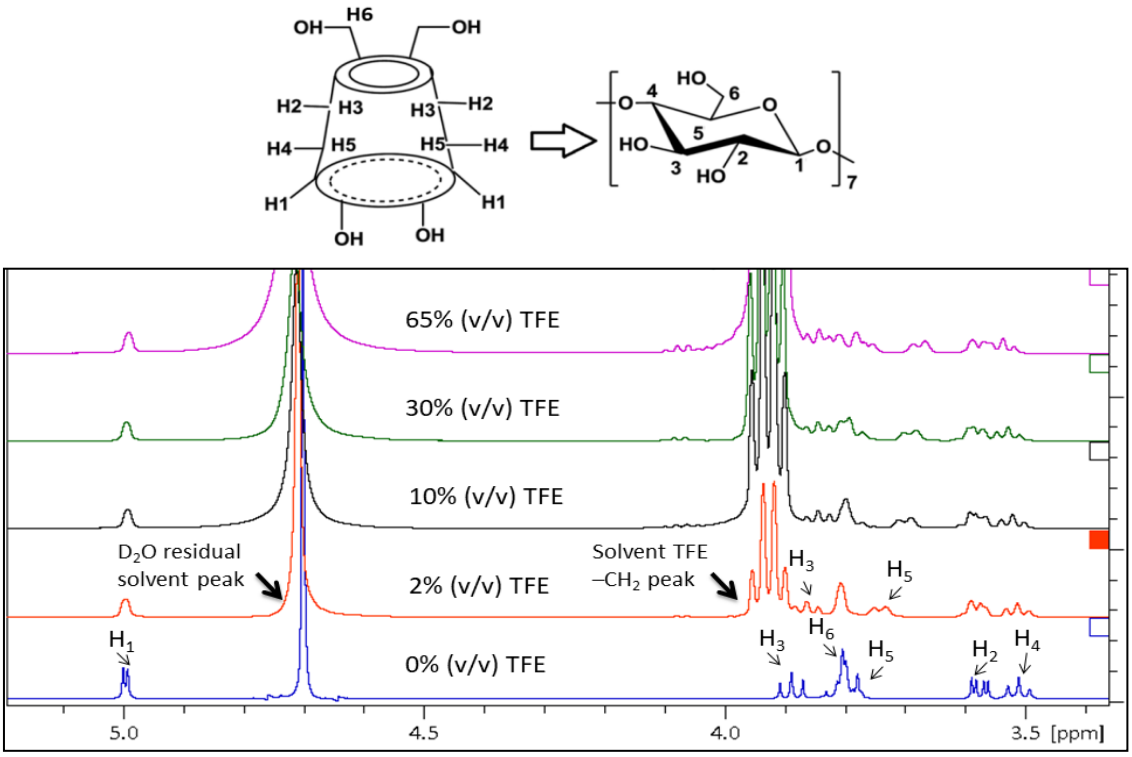

Figure 5.15: ^{1}H NMR spectra of β-CD in TFE: D_2O co-solvent mixture as a function of % (v/v) TFE composition at 298 K.

Further, the appearance of a single peak in the presence of carbohydrates *viz*., β-CD and glucose in both ^{2}H and ^{19}F NMR spectra also confirms that the solvent dynamics is under fast chemical exchange between two environments, namely bulk D_2O/TFE solvent and in the D_2O/TFE solvent molecules in the solvation sphere of carbohydrates [Beek et al., 1991]. The specific solvation dynamics around the carbohydrate can be investigated by monitoring the variation in nuclear spin relaxation due to intermolecular interactions between carbohydrate and solvent. We, therefore, attempt to measure the spin-lattice relaxation rates for the solvents both at high and low magnetic fields. It must be highlighted that for the first time ^{2}H and ^{19}F NMR spin-lattice relaxation rates (R_{1D} and R_{1F}) for D_2O and TFE are monitored and further analysed to extract the correlation times respectively to predict the co-solvent interaction behavior with solutes *viz*., β-CD and D-glucose.

(a) Analysis of longitudinal relaxation rate (R_1) ratio:

Table 5.6 reports the viscosities of the carbohydrate solutions while table 5.7 and 5.8 tabulates the relaxation rates of the solvents measured for these β-CD and glucose solutions respectively. It is clear from table 5.6 that the viscosity of TFE: D_2O co-solvent increases continuously with increase of % (v/v) of TFE. On the other hand for the same solvent compositions, the values of viscosity have shown an insignificant change with the addition of carbohydrates. Hence, any variation observed in the measured R_{1D} values of D_2O or R_{1F} values of TFE on addition of β-CD or glucose reflects the effect of interaction of the solvent molecules with that of the carbohydrate giving rise to formation of a solvation sphere around the carbohydrate resulting in to two different chemical environments for the solvents namely, the bulk solvent and solvent bound to the carbohydrate. Table 5.7 and 5.8 clearly demonstrates that in the absence of carbohydrates, an increase in ^{2}H D_2O (R_{1D}) and ^{19}F TFE (R_{1F}) spin-lattice relaxation rates are observed with increasing % (v/v) TFE that can be attributed to the increased viscosity of the solution.

Table 5.6: Viscosity of the solution (a) TFE: D_2O (b) 5 mM β-CD in TFE: D_2O (c) 5 mM glucose in TFE:D_2O and the calculated hydrodynamic radius (r_H) for β-CD and glucose from the viscosity and diffusion coefficient using Stoke-Einstein's' relation (equation 2.19, chapter 2) at 298 K.

%(v/v) TFE in D_2O	Viscosity (η) (mPa.s)	η *(mPas)* in presence of β-CD	η *(mPas)* in presence of Glucose	r_H (A°) β-CD	r_H (A°) *Glucose*
0%	1.306	1.318	1.310	5.34	2.53
2%	1.320	1.343	1.334	5.57	2.56
5%	1.425	1.438	1.430	5.76	2.60
10%	1.565	1.579	1.577	5.95	2.87
20%	1.861	1.876	1.870	6.26	2.99
30%	1.988	2.105	2.041	6.40	3.06
42%	2.203	2.250	2.220	6.52	3.10
65%	2.385	2.427	2.409	6.66	3.07
80%	2.050	2.120	2.052	6.85	3.11
95%	1.672	1.751	1.713	……	…….

Table 5.7: Values of measured relaxation rate, R_{1D} for D_2O and R_{1F} for TFE at 11.7 T. Extracted rotational correlation times (τ_c) from ^2H R_{1D} (11.7 T) and ^{19}F R_{1F} (0.34 T) for solvent D_2O and TFE respectively in absence and presence of 5 mM β–CD. τ_c* represent the value determined from solution viscosity only for D_2O.

%(v/v) TFE in D_2O	R_{1D} (s^{-1})	$\tau_{c(D)}$ *(ps)*	τ_c* *(ps)*	$R_{1F}{}^a$ (s^{-1})	$R_{1F}{}^b$ (s^{-1})	$\tau_{c(F)}{}^b$ *(ps)*
0%	2.14 ±0.03	2.15 ±0.03	2.14 ±0.04	--------	-------	-------
0%+β-CD	2.45 ±0.01	2.47 ±0.01	2.20 ±0.02	--------	-------	-------
2%	2.30 ±0.02	2.32 ±0.02	2.33 ±0.01	0.241 ±0.006	0.178 ±0.007	12.25 ±0.48
2%+β-CD	2.62 ±0.01	2.64 ±0.01	2.37 ±0.03	0.249 ±0.009	0.190 ±0.005	13.06 ±0.34
5%	2.49 ±0.02	2.51 ±0.02	2.51 ±0.03	0.252 ±0.005	-------	-------
5%+β-CD	2.73 ±0.04	2.75 ±0.04	2.53 ±0.05	0.269 ±0.007	-------	-------
10%	2.75 ±0.04	2.78 ±0.04	2.77 ±0.02	0.261 ±0.005	0.216 ±0.008	14.87 ±0.55
10%+β-CD	2.90 ±0.03	2.92 ±0.03	2.80 ±0.04	0.289 ±0.008	0.244 ±0.009	16.78 ±0.61
20%	3.26 ±0.05	3.28 ±0.05	3.29 ±0.04	0.294 ±0.004	0.222 ±0.005	15.28 ±0.34
20%+β-CD	3.28 ±0.06	3.30 ±0.06	3.31 ±0.05	0.339 ±0.007	0.261 ±0.005	17.96 ±0.34
30%	3.47 ±0.06	3.50 ±0.06	3.51 ±0.04	0.312 ±0.004	-------	------
30%+β-CD	3.44	3.48	3.71	0.357	-------	------

	±0.07	±0.07	±0.07	±0.006		
42%	3.86 ±0.08	3.89 ±0.08	3.89 ±0.05	0.339 ±0.003	0.303 ±0.003	20.85 ±0.20
42%+β-CD	3.81 ±0.07	3.83 ±0.07	3.97 ±0.09	0.359 ±0.004	0.327 ±0.006	22.51 ±0.41
65%	4.17 ±0.09	4.20 ±0.09	4.21 ±0.06	0.377 ±0.002	0.351 ±0.004	24.16 ±0.27
65%+β-CD	4.15 ±0.08	4.19 ±0.08	4.28 ±0.10	0.387 ±0.004	0.368 ±0.003	25.33 ±0.20
80%	6.06 ±0.10	6.12 ±0.10	6.35 ±0.07	0.610 ±0.006	------	------
80%+β-CD	6.21 ±0.11	6.26 ±0.11	6.80 ±0.010	0.611 ±0.007	-------	------

[a]: ^{19}F R_1 measurements at 11.7 T , [b]: ^{19}F R_1 measurements at 0.34 T ; T=298K.

Table 5.8: Values of measured relaxation rate, R_{1D} for D_2O and R_{1F} for TFE at 11.7 T. Extracted rotational correlation times (τ_c) from ^2H R_{1D} (11.7 T) and ^{19}F R_{1F} (0.34 T) for solvent D_2O and TFE respectively in absence and presence of 5 mM glucose. τ_c* represent the value determined from solution viscosity only for D_2O.

%(v/v) TFE in D_2O + 5 mM glucose	R_{1D} (s^{-1})	$\tau_{c(D)}$ *(ps)*	τ_c* *(ps)*	$R_{1F}{}^a$ (s^{-1})
0%	2.39±0.03	2.40±0.03	2.29±0.02	---------
2%	2.56±0.02	2.58±0.02	2.35±0.03	0.244±0.007
5%	2.65±0.01	2.67±0.01	2.52±0.05	0.262±0.007
10%	2.79±0.03	2.82±0.03	2.78±0.04	0.279±0.006
20%	3.23±0.04	3.25±0.04	3.30±0.06	0.324±0.004
30%	3.42±0.06	3.44±0.06	3.60±0.05	0.344±0.004
42%	3.79±0.08	3.82±0.08	3.92±0.08	0.353±0.002
65%	4.17±0.09	4.20±0.09	4.25±0.07	0.385±0.003
80%	6.16±0.11	6.22±0.11	7.23±0.08	0.609±0.006

It must be pointed out that the measured spin-lattice relaxation rates for the solvent molecules in presence of the carbohydrate are a weighted average of the relaxation rates of the solvents in the bulk and within the solvation sphere. To nullify the effect of viscosity on the relaxation rates, R_1 ratio measured for solvents in presence and absence of carbohydrate is analyzed. Such a ratio of R_1 for D_2O and TFE are plotted as a function of % (v/v) of TFE in figure 5.16. The ratio of R_{1D} *or* R_{1F} greater than 1 suggests that the R_1 either for D_2O or for TFE has increased with the addition of the carbohydrates compared to that of the free solvent molecules. Hence any increment in R_1 value is a result of the interaction of the carbohydrates with the solvent molecules. One would expect that bulk solvent molecules to be experiencing faster molecular motions similar to the solvent molecules in absence of the solute (R_{1Free}). On the other hand the solvent molecules immediately in the vicinity of the solute will experience a comparatively slower motion due to a structured solvation sphere indicating interaction with the solute.

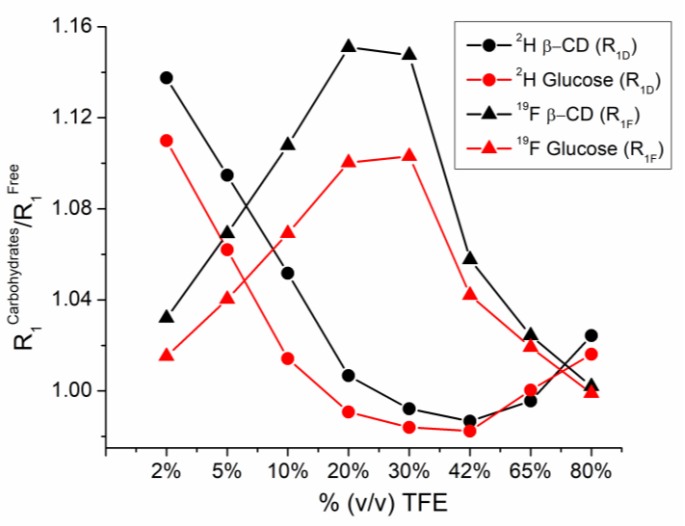

Figure 5.16: R_{1D} and R_{1F} ratio for D_2O (^{2}H-circle) and TFE (^{19}F-triangle) respectively in the presence of (a) β-CD (black) and (b) glucose (red) to free co-solvent mixture (without carbohydrates) as a function of % (v/v) TFE composition in D_2O at 298 K.

A closer inspection of figure 5.16 reveals the following points:
(i) R_{1F} ratios for both the carbohydrates increase progressively with increasing % (v/v) TFE composition up to 30%, and decreases afterward for 42% to 80% (v/v) TFE range.
(ii) R_{1D} ratios for both the carbohydrates drop with an increasing % (v/v) TFE composition. The sharp decrease in the ratio is observed at lower TFE concentration (up to 30%). Afterwards, the ratio is found to be similar in the range of 42% to 80% (v/v) TFE.
(iii) The changes in R_{1D} and R_{1F} ratio are seen higher for β-CD compared to that of the glucose up to 30% (v/v) TFE composition.

The first observation **(i)** can be attributed to the replacement of bound water molecules by TFE followed by the transfer of the water molecules to the bulk solvent in the range of 2% to 10% (v/v) TFE. TFE competes with D_2O to enter the immediate solvation sphere of carbohydrates. The ratio increases as more and more TFE enters the solvation sphere of carbohydrates causing the weighted average value of R_{1F} to be governed by TFE molecules within the solvation sphere directly interacting with the carbohydrate. The observation of maximum R_{1F} ratio from 20% to 30% (v/v) TFE possibly suggests that TFE has replaced almost all the water molecules from the solvation sphere of carbohydrates. The second **(ii)** observation corroborates the findings of the first observation. The addition of TFE reduces the number of water molecules by replacing them from the immediate solvation sphere of carbohydrates. Therefore, number of free water molecules possessing greater mobility is increased in the bulk solvent system compared to bound water molecules in the solvation sphere. Since the measured R_{1D} is a weighted average of the relaxation rates of D_2O in bulk and in solvation sphere, the ratio of R_{1D} in presence of carbohydrate to that in absence of carbohydrate decreases with increase of TFE concentration indicating replacement of D_2O from the solvation sphere of the carbohydrate.

Thereby, it can be commented that both the carbohydrates tend to undergo preferential solvation by TFE over water molecules. Also, the higher values of the R_{1F} ratio are seen at lower TFE percentages (below 42%) where TFE clustering is prevalent according to various previous studies on TFE: D_2O co-solvent mixture. It is already discussed in literature that TFE acts as a nanocrowder at lower concentrations [Culik et al., 2014]. In the present case, TFE causes preferential solvation by excluding volumes of water that are present in the solvation sphere and are in contact with the carbohydrates. At higher concentrations of TFE, the possibility of crowding is decreased as the co-solvent system becomes more homogenous in terms of TFE

[Culik et al., 2014]. As a consequence it causes an infinitesimal change in the R_{1D} and R_{1F} values of the solvent upon the addition of carbohydrates (respective R_1 ratio tends to 1) beyond 30% (v/v) TFE composition, as stated in observations i) and ii). The majority of TFE and nearly all D_2O molecules experience bulk behaviour similar to the co-solvent mixtures without carbohydrates making the changes in R_{1D} or R_{1F} ratio due to the preferential solvation of TFE over D_2O less obvious to be observed.

Observation **iii)** reflects the higher affinity of β-CD to undergo preferential solvation by TFE than the glucose molecules. It may be envisaged that in addition to solvation, β-CD can encapsulate TFE molecules in its cavity forming β-CD: TFE inclusion complexes. Such inclusion process will definitely slow down the mobility of the TFE molecules causing a greater change in R_1 ratio. The event of encapsulation is also supported by the ^{1}H NMR spectrum of β-CD (shown in figure 5.15) where the inner cavity protons (H_5) exhibited maximum changes in chemical shift and line-broadening compared to the outer rim protons (H_2) in presence of TFE as discussed earlier. The said observation is in accordance with the literature that confirms the inclusion of TFE within β-CD cavity [Guerrero-Martínez et al., 2006]. A point to be mentioned that after 80% (v/v) TFE, the carbohydrate samples appeared turbid. It can be explained that at higher TFE co-solvent composition the carbohydrates become insoluble.

(b) Determination of correlation time:

Measurement of R_1 enables the extraction of molecular rotational correlation times (τ_c) that can quantify the dynamics of solute-solvent interaction. In this section we have extracted the τ_c in absence and in the presence of carbohydrates for both D_2O ($\tau_{c(D)}$) and TFE ($\tau_{c(F)}$), the former at 11.7 T and the latter at 0.34 T.

In solution deuterium quadrupolar interaction is the major contributing relaxation mechanism causing ^{2}H relaxation. The motional modulation of the interaction between the quadrupole moment of ^{2}H and the electric field gradient at the nucleus causes a far superior relaxation process compared to any other relaxation mechanism such as dipolar interaction, chemical shift anisotropy and cross-relaxation. Hence, the interpretation of ^{2}H relaxation is less prone to error, in comparison to ^{1}H and ^{19}F, where multiple relaxation mechanisms are active at high magnetic field. In addition, unlike ^{19}F relaxation, cross-correlation mechanisms are negligible for ^{2}H, further simplifying the interpretation in motional terms [Bose-Basu et al., 2000; Sidhu et al., 1995]. ^{2}H R_1 for molecules tumbling isotropically in region of extreme motional narrowing is described by equation 5.3 [Abragam, 1961].

$$R_{1D} = \frac{1}{T_{1D}} = \left(\frac{3\pi^2}{10}\right)\left(1+\frac{1}{3}\eta_a^{\,2}\right)\frac{(2I+3)}{(I^2(2I-1))}(e^2qQ/h)^2\tau_{c(D)} \quad \text{....(5.3)}$$

Here, (e^2qQ/h): quadrupole coupling constant = 258.6 kHz for D_2O, η_a: the asymmetry parameter= 0.1 and hence the term $(1+1/3\,\eta_a^2)$ can be equated to 1 [Bhattacharjee et al., 1991; Hindman et al., 1971; Lankhorst et al., 1982]. $\tau_{c(D)}$ extracted from R_{1D} values for D_2O are reported in table 5.7 in absence and presence of β-CD as a function of % (v/v) TFE and similarly for glucose in table 5.8 .

The viscosities of the samples are known to affect the measured relaxation rates and hence, the extracted τ_c values. Therefore, the expected τ_c^* for D_2O due to solvent viscosity is also calculated following equation 5.4 (from viscosity value only) and is reported in table 5.7 for the β-CD system. While for the glucose system, similar data has been presented in table 5.8. τ_c^* represents the upper limit of correlation time that is possible due to a change in viscosity [Nanny and Maza, 2001].

$$\tau_c^* = \frac{4\pi f a^3}{3k_B T}\eta \ldots (5.4)$$

Here, *f*: micro-viscosity factor for a heterogeneous solvent mixture accounting the fact that diffusing molecule do not experience continuous medium, *a*: molecular radius of D_2O = 2.75 Å, k_B : Boltzmann constant, T: temperature.

It can be seen from table 5.7 and 5.8 that the extracted $\tau_{c(D)}$ for D_2O in the presence of carbohydrates during initial additions of TFE (upto 10%) from equation 5.3 is always higher than the expected increase in correlation time (τ_c*) due to viscosity of the sample from equation 5.4. Hence, it confirms that the solvation of carbohydrates by D_2O molecules must be a factor that leads to an additional increase in $\tau_{c(D)}$ values beyond the expected value based on solvent viscosity. As the concentration of %(v/v) TFE increased, the calculated $\tau_{c(D)}$ value from R_1 is in the range estimated from viscosity (τ_c *) confirming the previous observations that beyond 10% (v/v) TFE, nearly all D_2O molecules are replaced by TFE from the solvation sphere of β-CD. Similar observations are seen for the glucose system as well. The ratio of $\tau_{c(D)}$ in the presence of carbohydrates to $\tau_{c(D)}$ of free co-solvent mixture (figure 5.17) coincides with the trends of R_{1D} ratio seen in figure 5.16 supporting the aforesaid discussions related to relaxation rate of ^2H of D_2O.

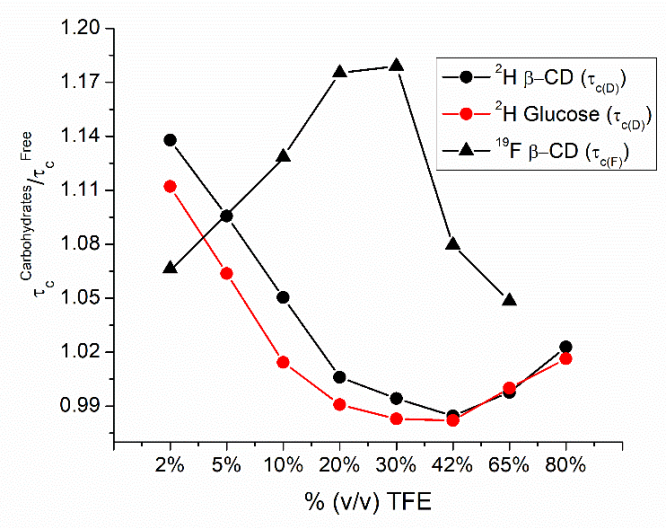

Figure 5.17: $\tau_{c(D)}$ and $\tau_{c(F)}$ ratio for D_2O (^2H-circle) and TFE (^{19}F-triangle) respectively in presence of (a) β–CD (black) and (b) glucose (red) to free co-solvent mixture (without carbohydrates) as a function of %(v/v) TFE composition in D_2O at 298K.

For TFE, the extraction of correlation time at high field is a cumbersome affair due to the presence of dipolar as well as CSA based relaxation mechanisms as discussed in Part I. There are two ways to overcome this hurdle: i) one may measure the ^{19}F R_1 values at considerably low magnetic field that ensures CSA to be inactive and ii) to measure the TFE correlation time by either measuring the ^{13}C R_1 or ^2H R_1 for deuterated TFE. In the present case, we chose to measure the ^{19}F R_1 values at low field, *i.e.*, *ca.* 0.34 T similar to Part I to avoid the complexities arising from CSA relaxation contribution that limits the determination of τ_c values for TFE at 11.7 T. Following the set of reasonable assumptions (discussed in part-I section: 5.3.1 ii (a)), the ^{19}F τ_c values for TFE ($\tau_{c(F)}$) are determined from low field ^{19}F R_1 values using equation 5.1 [Abragam, 1961; Solomon, 1955].

$\tau_{c(F)}$ values for TFE increases in the presence of β-CD and the $\tau_{c(F)}$ ratio followed the same trend as seen for R_{1F} ratio in figure 5.16. Hence, the same explanation of R_{1F} ratio can be presented for $\tau_{c(F)}$ ratios (figure 5.17). A point to be mentioned here that R_{1F} values at 0.34 T are smaller than R_{1F} at 11.7 T due to reduced contribution from CSA. Also, the R_{1F} ratio of TFE in the presence of β-CD to free TFE at 0.34 T are comparatively of greater magnitude than that of R_{1F} ratio at 11.7 T making the low field measurements for ^{19}F system to be more sensitive towards assessing molecular dynamics.

(c) Supporting experimental data corroborating preferential solvation:

It must be pointed out here that the changes seen in R_1 values of solvent (D_2O, TFE) are of small magnitude as the measurements are made for only 5 mM concentration of carbohydrates (due to the limited solubility of β-CD). Therefore, to eliminate any misleading information provided by solvent R_1 measurement analysis regarding the solvation phenomenon of the carbohydrates, the ^1H self-diffusion coefficients (D) for solute molecules are determined using BPPLED pulse sequence shown as figure 2.12 in chapter 2. Further, the hydrodynamic radii (r_H) of the solutes are determined following Stoke-Einsteins relation given by equation 2.19 (chapter 2, section 2.5). The same has been presented in table 5.6. The r_H values for carbohydrates show an increase in magnitude with increasing %(v/v) TFE concentration that confirmed the preferential coating [Fioroni et al., 2002] of the carbohydrate surface by TFE. The close inspection of table 5.6 reveals that the sizes of the both the carbohydrates exhibit an overall tendency to increase with increasing TFE composition than in pure water. At high TFE concentrations (>10% TFE) sizes of both the carbohydrates become significantly larger than in water. These findings can be interpreted as preferential coating of the carbohydrates molecules by TFE in the TFE: D_2O co-solvent mixtures that cover effectively the surface of carbohydrates increasing their "apparent size". Also, the increase in β-CD size is of higher extent than that of the glucose. This suggest enhanced tendency of β-CD to undergo preferential solvation by TFE.

5.4 CONCLUSIONS

The present chapter undoubtedly demonstrates the applicability of ^{19}F spin-lattice relaxation measurements conducted at low magnetic field to be a viable method that unveils the motional behaviour of the fluorinated solvent as an indirect probe to analyse the solute-solvent interaction in solution in conjunction with low field ODNP measurements (Part I) and high field ^2H spin-lattice relaxation rates (Part II). The chapter highlights the ease of determination of τ_c at low magnetic field that can reveal motional behaviour of solvents in presence of particular solute molecules. Both Part I and Part II of the current chapter utilizes the fact that at low magnetic field, CSA contribution as a relaxation mechanism for ^{19}F can be nullified resulting in a straightforward extraction of τ_c. Moreover, the motional regime experienced by the solvent molecules is always in the extreme narrowing region. Low field ^{19}F R_1 measurements allow fast acquisition as compared to that of natural abundance ^{13}C R_1 at high field besides omitting the requirement of deuterium labelling of fluoro-solvents for ^2H R_1 measurements at high magnetic field.

The major outcome of Part I are summarized here under:

1. Low field ^{19}F R_1 measurements in conjunction with low field ODNP experiments provide a robust approach to decipher solvation behaviour of fluorinated solvents around conformationally dynamic macromolecules; MLT in specific.
2. Routine high field R_1 and diffusion data recorded for MLT or TFE are inconclusive to infer dynamical interaction between TFE and MLT.
3. TFE concentrates around MLT and interacts directly with MLT irrespective of the pH conditions. It tends to stabilize open helical structures whether MLT is initially present in tetramer (set-I) or in random coiled form (set-II). TFE imparts such stabilization by surrounding MLT or residing on MLT surface.

4. The relaxation rate of TFE in presence of MLT for both the sets has a differential dependence on TFE percentage (2−65%). In particular, the maximum change in TFE relaxation rate in presence of MLT occurs at low TFE percentage (below 42%) where TFE clustering is also prevalent. At higher concentrations of TFE, the co-solvent system becomes more homogenous that reduces the possibility of crowding.
5. TFE probably acts as a nano-crowder and follows a similar mechanism of increasing alpha helicity of peptide through the excluded volume effect already discussed in literature [Culik et al., 2014].

The major highlights of Part II as are follows:

1. Successful demonstration of a unique combination of solvent ^{2}H and ^{19}F R_1 measurements at high and low magnetic field respectively is accomplished for the analysis of TFE: D_2O co-solvent dynamics during the preferential solvation of carbohydrates.
2. Both the carbohydrates used in the analysis prefer to undergo solvation by TFE over D_2O. The maximum solvation by TFE occurs in 20%-30% (v/v) TFE composition for both the cases.
3. The straightforward determination of τ_c from high field ^{2}H R_{1D} and low field ^{19}F R_{1F} simplifies the quantification of the molecular mobility and supports the findings from R_1 ratio trends. This method can be extrapolated to study the solvation dynamics of large molecular systems where substantial changes in R_1 values can be observed.

In a nutshell these set of analysis definitely open up viable options to decipher molecular dynamics in the solution-state solely through analysis of solvent dynamics.

….